Low-frequency atomic stabilization and dichotomy in superintense laser fields: Full Floquet results

M. Stroe,[1] I. Simbotin,[2] and M. Gavrila[2,3]
[1]*Department of Chemistry, University of Bucharest, R-030018 Bucharest, Romania*
[2]*Institute for Theoretical Atomic and Molecular Physics, Harvard-Smithsonian Center for Astrophysics, Cambridge, Massachusetts 02138, USA*
[3]*FOM Institute for Atomic and Molecular Physics, 1098 SJ Amsterdam, The Netherlands*
(Received 23 April 2008; published 8 September 2008)

In the preceding paper we have shown, based on the high-intensity, high-frequency Floquet theory (HIHFFT), that atomic quasistationary stabilization (QS) and dichotomy are not necessarily high-frequency phenomena as widely believed, but can occur also at photon energies small with respect to the unperturbed ground state binding energy, provided that the field is strong enough. In this paper we approach the issue from the point of view of accurate numerical Floquet computations. We have made a comprehensive determination of the Floquet quasienergies for a one-dimensional (1D) atomic model with a soft-core Coulomb potential (ground state energy $W_0=-0.500$ a.u.) in a laser field of constant amplitude E_0 and frequency ω. The excursion parameter $\alpha_0=E_0/\omega^2$ was varied over the range $0<\alpha_0<100$, at two low frequencies $\omega=0.12$ and 0.24 a.u. ($\omega<|W_0|$); the lowest-lying 18 states were computed. We present graphs for the α_0 dependence of the energies of the states in the field, $W(\alpha_0)=\mathrm{Re}\,E$ ("Floquet maps"), and their ionization rates $\Gamma(\alpha_0)$. An intricate behavior of $W(\alpha_0)$ was revealed at low α_0, with many crossings, avoided crossings (ACs), and Floquet states materializing or disappearing at multiples of ω energy thresholds. At large α_0, however, the uneventful pattern encountered at high frequencies is regained, in which the levels tend monotonically to zero modulo ω (i.e., the binding energies of all states vanish). Also $\Gamma(\alpha_0)$ varies substantially at low α_0, attaining sometimes large values, but at large α_0 it decreases to zero in an oscillatory manner (QS). The form of the components of the Floquet wave function was also followed from low to large α_0, and abrupt changes were found in most cases at ACs. The Floquet results were then compared to a computation of the HIHFFT formulas for the quasienergies and good agreement was found (to within the expected accuracy of HIHFFT). This confirms that HIHFFT is fully capable of describing the low-frequency regime at large enough α_0, and in particular the existence of QS and dichotomy.

DOI: 10.1103/PhysRevA.78.033405 PACS number(s): 32.80.Rm, 42.50.Hz

I. INTRODUCTION

It has been widely assumed that atomic dichotomy and stabilization in intense laser fields are high-frequency phenomena, occurring at frequencies ω of the order of the unperturbed binding energy of the ground state, or higher (for a review, see [1]). Practically all calculations done either for quasistationary stabilization (QS) via the Floquet approach, or for dynamic stabilization (DS), via the time-dependent Schrödinger equation approach, pertain to this case. The idea may have originated in the fact that QS was derived using the high-frequency Floquet theory (HFFT) (see [2,3]). However, in the preceding paper [[4], referred to as I] we have shown that this was not the case, as QS and dichotomy can occur also at arbitrarily low frequencies, provided that the field strength E_0 is sufficiently high. This was done by showing that the iteration procedure of HFFT for the quasienergies and wave functions converges also in the latter regime. Thus, a more adequate designation of the theory should be high-intensity, high-frequency Floquet theory (HIHFFT). In I we have illustrated the general three-dimensional (3D) results with the case of a 1D soft-core Coulomb potential model, for which explicit analytic formulas could be obtained from the general HIHFFT results.

In this paper, we approach the problem of the low-frequency regime ($\omega<|W_0|\equiv$ unperturbed ground state binding energy) from the numerical Floquet point of view. We have computed accurately the quasienergies and eigenfunctions of the Floquet system of differential equations for the aforementioned 1D model at the low frequencies $\omega=0.12$ and 0.24 a.u. ($|W_0|=0.500$ a.u.), over an extended range of field values E_0, and for many (18) low-lying states. In terms of the classical excursion parameter $\alpha_0=E_0\omega^{-2}$ a.u. we are using, the range covered was $0<\alpha_0<100$. This comprehensive overview allowed us to establish a correlation between the low- and large-α_0 behavior [5]. The results for the α_0 dependence of $W\equiv\mathrm{Re}E$ are presented in graphs that we have termed Floquet maps. More recently, such maps have been obtained in [6] for the 3D case of Ar modeled by a radial potential ($\alpha_0<13.8$).

The paper is organized as follows. The numerical methods used are described in Sec. II. The relevant HIHFFT analytic formulas for the quasienergies and eigenfunctions of the 1D model derived in I are briefly recalled in Sec. III. These formulas were obtained from the general HIHFFT results by making the large-α_0 assumption. They provide more transparency concerning the physical interpretation but, on the other hand, are limited by this assumption. In Sec. IV we present our Floquet results for the quasienergies E. The Floquet maps obtained for $W\equiv\mathrm{Re}\,E$ reveal a complexity of level crossings and avoided crossings (ACs) at low α_0. These are shown in Sec. V to be related to changes in the nodal

structure of the components of the Floquet wave function. Conclusions and perspectives are presented in Sec. VI. Our numerical results confirm the predictions of HIHFFT obtained in I.

Some remarks are in place. Our results pertain to individual Floquet states. The connection of the mathematical Floquet states with the physics can be done in two ways. Under the assumption that one is dealing physically with long, quasimonochromatic pulses, with adiabatically varying amplitudes, one can attempt to describe the situation by a single Floquet state ("single-state Floquet theory"). Our results apply directly to this case. In the case of short, superintense pulses it is necessary to resort to "multistate Floquet theory," which is based on the mathematical possibility of describing wave packets as superpositions of Floquet states (see [7–9] and references therein). In this context, Floquet maps are an important auxiliary in following the time evolution of the atom because they can serve to identify its evolution along diabatic paths. These paths consist of successions of Floquet states contained in the wave packet decomposition, along which the atom preferentially evolves, with quantal jumps at ACs (see, for example, [10], and also [11,12]). Comprehensive information on Floquet states allows a physical understanding of atomic dynamics in the field, complementary to that obtained by the direct numerical integration of the time-dependent Schrödinger equation.

II. 1D MODEL AND COMPUTATIONAL METHODS

In this paper we use the 1D model with soft-core Coulomb potential

$$V(x) = -\frac{1}{\sqrt{a^2 \exp[-(x/a)^2] + x^2}}. \tag{1}$$

At large $|x|$, this has a Coulomb tail supporting an infinite set of Rydberg states. The term $a^2 \exp[-(x/a)^2]$ under the square root "softens" the $1/|x|$ singularity at the origin, which is too strong for a consistent mathematical treatment in the 1D case. The exponential multiplying a^2 was introduced for numerical convenience (see [16]). We have chosen $a=1.6$ so that the ground state energy is $W_0=-0.500$ a.u.

Floquet computations endeavor to solve the differential system of equations

$$[H-(E+n\omega)]\phi_n(x) = -\sum_{m}^{(m\neq n)} V_{n-m}(\alpha_0;x)\phi_m(x), \tag{2}$$

where $\phi_n(x)$ are the components of the Floquet solution $\psi(x,t)=e^{-iEt}\Sigma_n \phi_n(x)e^{-in\omega t}$. Here,

$$H \equiv \frac{1}{2}P^2 + V_0(\alpha_0;x), \tag{3}$$

and $V_m(\alpha_0;x)$ are the Fourier components of the oscillating potential $V(x+\alpha_0 \mathbf{e}\cos t)$:

$$V_m(\alpha_0;x) = \frac{1}{2\pi}\int_0^{2\pi} e^{im\chi} V(x+\alpha_0\cos\chi)d\chi. \tag{4}$$

Boundary conditions of the Gamow-Siegert type are imposed to obtain Floquet ionizing states (see I, Sec. II A). They can be expressed in general both for a Columb-type potential as in Eq. (1) with asymptotic charge $Z=1$, and for a short-range potential with asymptotic charge $Z=0$, as

$$\phi_n^{(P)}(x) \to \begin{cases} f_n \exp(i\theta_n) & \text{for} \quad x\to+\infty, \\ (-1)^{P+n} f_n \exp(-i\theta_n) & \text{for} \quad x\to-\infty, \end{cases} \tag{5}$$

where $\theta_n = k_n|x| + Zk_n^{-1}\ln 2k_n|x|$, and k_n is obtained from $k_n^2/2 \equiv (E+n\omega)$, with the choice of the square root depending on if the channel is open or closed, according to

$$\mathrm{Re}k_n < 0, \quad \mathrm{Im}\, k_n > 0, |\mathrm{Re}k_n| < \mathrm{Im}\, k_n \quad \text{(closed channels)}, \tag{6}$$

$$\mathrm{Re}k_n > 0, \quad \mathrm{Im}\, k_n < 0, \quad \mathrm{Re}k_n > |\mathrm{Im}\, k_n| \quad \text{(open channels)}. \tag{7}$$

By imposing the boundary conditions Eqs. (6) and (7), the problem becomes an eigenvalue problem for the determination of the complex quasienergy $E \equiv W - i(\Gamma/2)$.

The numerical program used to solve Eq. (2) was described for the 1D short-range potential case ($Z=0$) in [13], Sec. III. It proceeds by truncating the system of coupled equations (2) to a number N, sufficiently large to ensure the accuracy desired. N linearly independent solutions $\psi^{(j)}$ (with N components) are generated by requiring that, at $x\to+\infty$, $\psi^{(j)}$ behaves as $f_j \exp(i\theta_j)$ in channel j and vanishes in all others. A complex trial value E_t is chosen for the quasienergy in the expression of k_n, the same for all $\psi^{(j)}$. The solutions $\psi^{(j)}$ are then propagated inward with the Numerov algorithm. The desired Ψ_E is a linear combination of the N solutions $\psi^{(j)}$. In order that Ψ_E satisfy the boundary condition Eq. (5) also for $x\to-\infty$, and thereby become an eigensolution, it needs to have definite parity P. This is imposed in the vicinity of the origin by extending the integration one step into the $x<0$ interval, i.e., to grid point $-h$, and comparing Ψ_E at grid points $\pm h$. A determinantal compatibility condition appears for E_t, which in general will not be satisfied for the arbitrarily chosen E_t. A fast optimization routine is applied iteratively to select an improved value for E_t, until the condition is satisfied by the correct E. To keep the memory requirements low, we did not store the solutions $\{\psi^{(j)}\}$ during the computation.

Because of the special nature of the boundary conditions (open channel Floquet components increase exponentially at infinity, whereas closed channels decrease exponentially), during propagation the N solutions tend to become linearly dependent, leading to numerical instability. In order to avoid this, a number of linear transformations are applied to the set of solutions $\{\psi^{(j)}\}$ along the way. For details, see [13], Sec. III.

As the $\{\psi^{(j)}\}$ were not stored during the computation of E, in order to determine $\Psi_E^{(P)}$, the program is run once again with this E as a trial value. Now the parity condition at the origin allows the determination of their linear combination, yielding $\Psi_E^{(P)}$. As the components of $\Psi_E^{(P)}$ satisfy Eq. (2) with boundary conditions Eqs. (5)–(7), it is indeed the quasienergy solution.

The program was extended to the Coulomb-tail potential case ($Z=1$) by one of us [14]. Because of the long-range

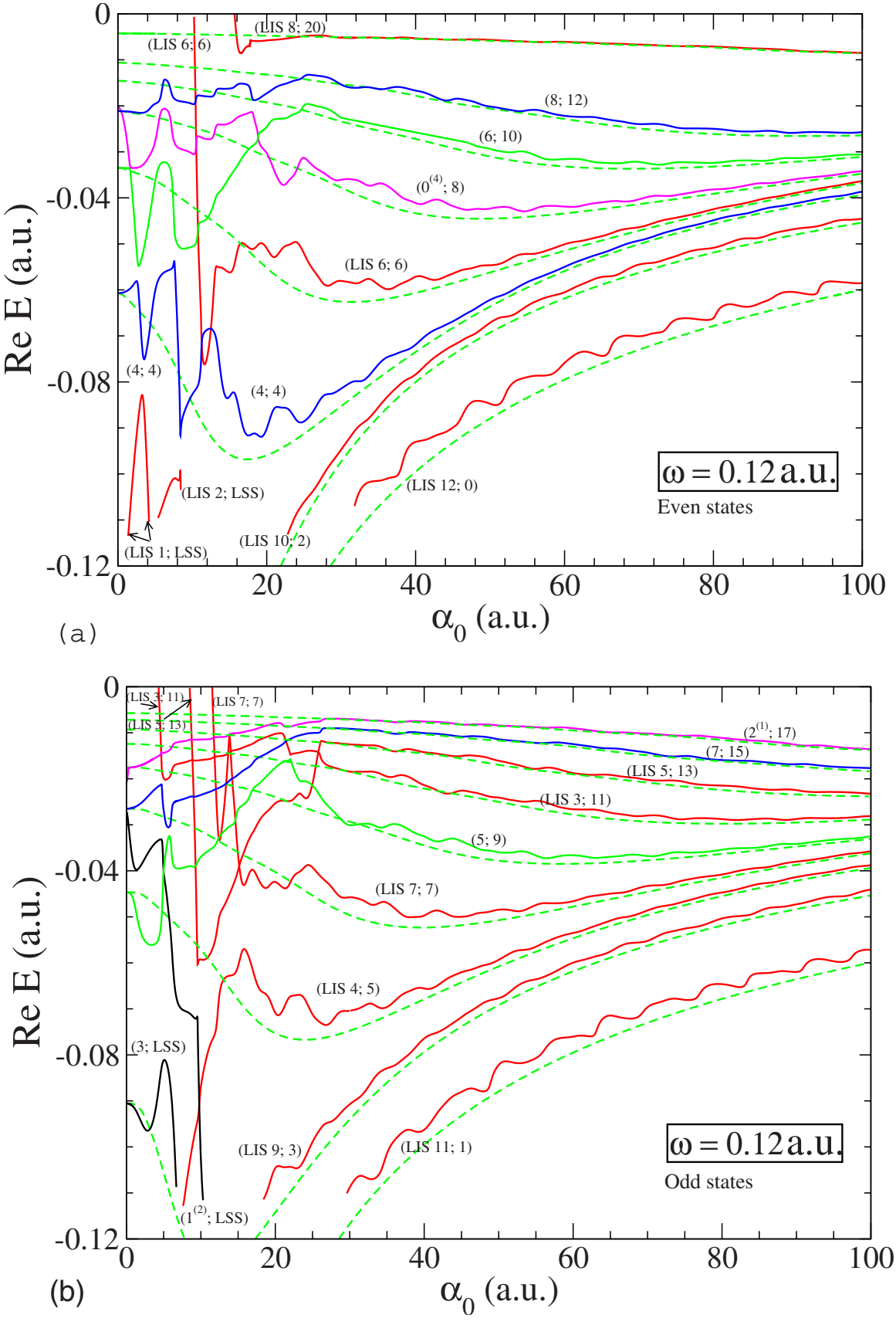

FIG. 1. (a) (Color online) Real part of Floquet quasienergies for the even states of the 1D model Eq. (1) at ω=0.12 a.u. (full lines). Corresponding eigenvalues $W(\alpha_0)$ of the 1D HIHFFT structure equation (10) (dashed lines). Floquet states are characterized by the notation $(n;\nu)$ described in Sec. IV C. (In color, LISs are drawn in shades of red and LSSs in black.) (b) Same as (a) except for odd states.

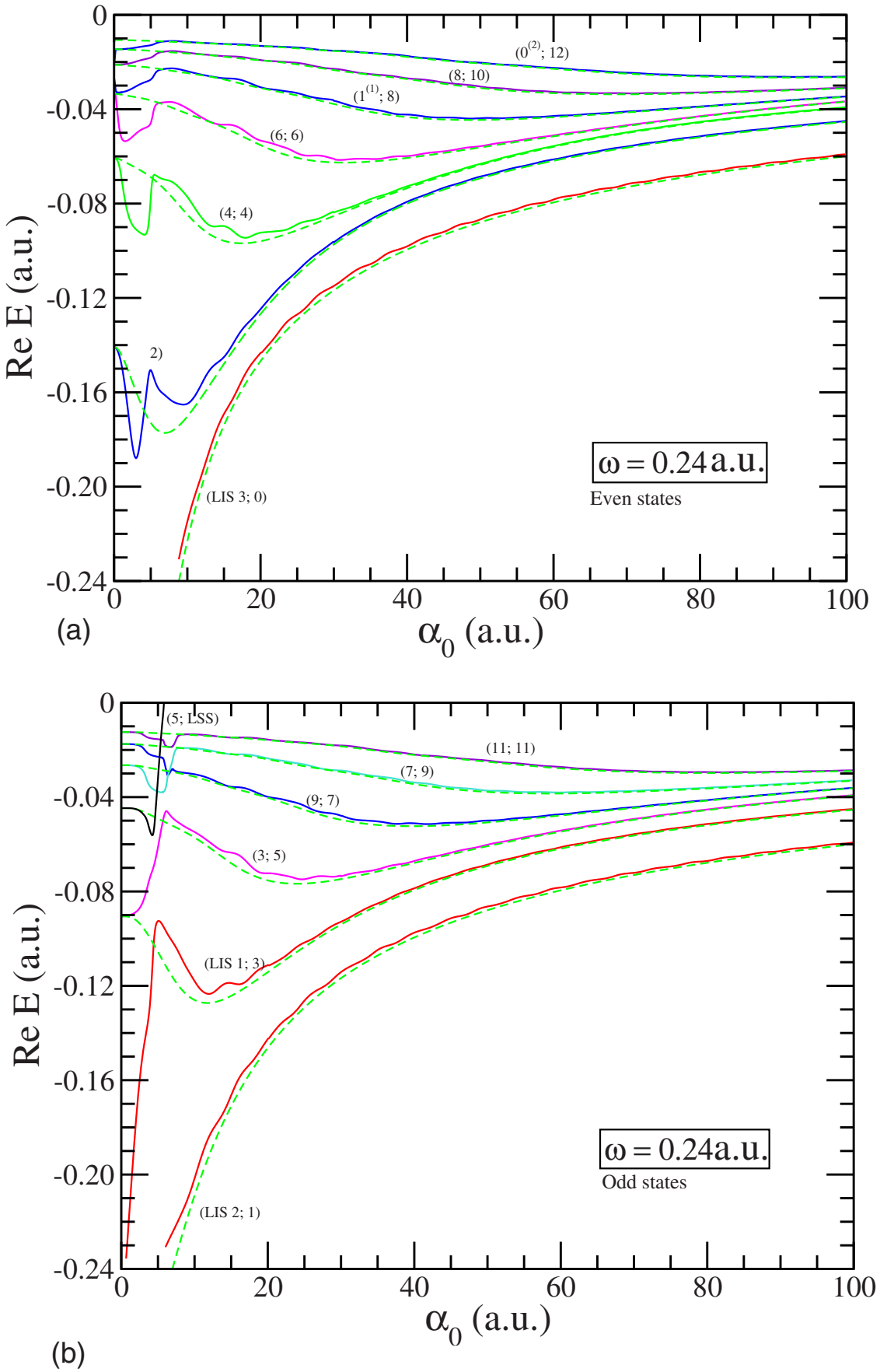

FIG. 2. (Color online) (a) Same as Fig. 1(a), except that ω=0.24 a.u. (b) Same as for Fig. 1(b), except that ω=0.24 a.u..

nature of the potential, the asymptotic form Eq. (5) is attained very slowly. The problem was to find an improved form so as to enter the asymptotic regime at a smaller value x_0. (A similar problem appears in scattering theory, see [15], Sec 1.4.4.) To this end, the Fourier coefficients $V_n(x)$, Eq. (4), were expanded in powers of $1/x$, as

$$V_n(x) = \frac{1}{x}\sum_{\lambda \geqslant n} b_n^\lambda \left(\frac{\alpha_0}{x}\right)^\lambda \quad (x \gg \alpha_0), \tag{8}$$

where b_n^λ are constants, and one can take $n>0$ as $V_{-n}=V_n$; note that $\lambda \geqslant n$. We then write similar expansions for the N linearly independent solutions of interest:

$$\Phi^{(j)} \equiv (\Phi_n^{(j)}(x)), \quad \Phi_n^{(j)}(x) \equiv \sum_{p=0} \frac{1}{x^p}\sum_q a_{pq}^{(j)n} e^{i\theta_q},$$

$$j = 1, \ldots, N, \tag{9}$$

with starting conditions $a_{pq}^{(j)n} = \delta_{p0}\delta_{nj}\delta_{qn}$. The sum over q runs over all N channels, and allows for asymptotic channel coupling. By inserting the series for $V_n(x)$ and $\Phi_n^{(j)}(x)$ in Eq. (2) and equating the coefficients of equal powers of x^{-1} on the left- and right-hand sides, a system of algebraic recurrence relations is obtained for the $a_{pq}^{(j)n}$ of fixed j. The starting conditions allow the unique determination of $a_{pq}^{(j)n}$. Equation (9) then gives the improved form of the asymptotic condition for each $\Phi^{(j)}$. However, as in the short-range case, the Floquet eigenfunction $\Psi_E^{(P)}$ is a linear combination of the $\Phi^{(j)}$ with unknown coefficients. These are again determined at the origin by imposing the parity condition.

One needs to make a compromise concerning the point x_0 where one applies the asymptotic procedure, so that, on the one hand, it be sufficiently large for the Coulomb asymptotic formula Eq. (9) to be accurate enough, and, on the other hand, it be sufficiently small in order that the exponential increase imposed by the Gamow-Siegert boundary conditions be minimal [16]. At that point x_0, there is an optimal number of terms to be taken in the $1/x$ expansions for best accuracy, because the expansions are asymptotic.

Proceeding along the lines described a very stable program has emerged, even at large values of α_0. (The latter case is more difficult because the size of the atom, and hence of the grid required, increases with α_0; see Sec. III.) Nevertheless, not all light-induced states (LISs) in the Floquet maps, could be determined in the vicinity of their materialization point α_0, e.g., the states denoted as (LIS 10;2), (LIS 12;0) in Fig. 1(a), (LIS 9;3), (LIS 11;1) in Fig. 1(b), (LIS 3;0) in Fig. 2(a), and (LIS 2;1) in Fig. 2(b). This is because, due to an interplay of the parameters, the recurrence relations used in connection with the asymptotic integration tend to break down in these cases in the vicinity of the materialization thresholds. For the same reason, we could not continue light-suppressed states (LSSs) to their disappearance thresholds, e.g., (3; LSS) and ($1^{(2)}$; LSS) in Fig. 1(b).

On the other hand, the program has permitted us to calculate some of the shadow states giving rise to the LISs we have found. By this we mean that we could follow continuously in α_0 below the materialization threshold of a particular LIS the Floquet solution giving rise to it (see I, Sec. II A).

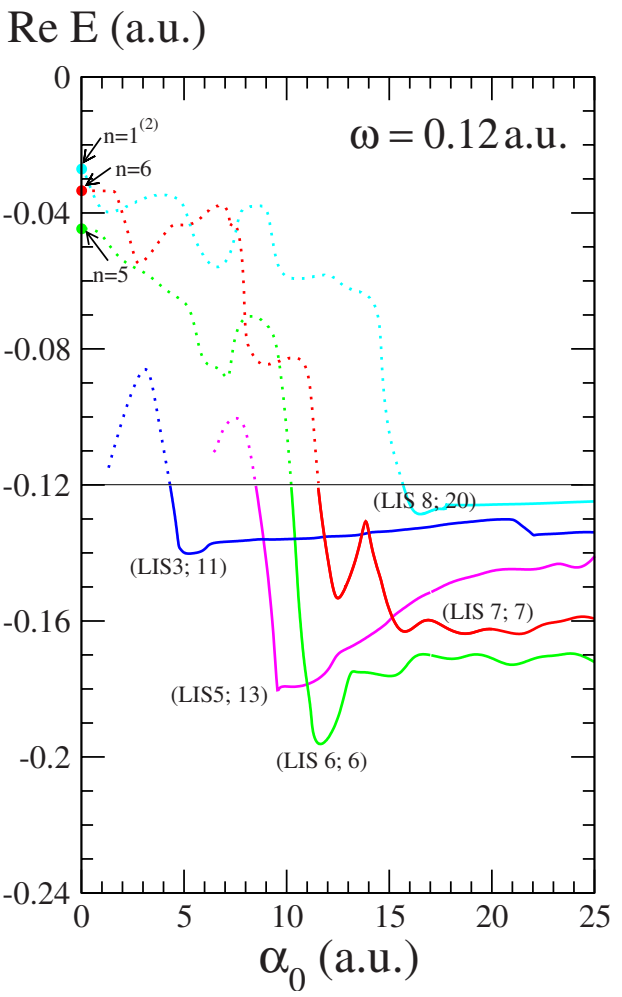

FIG. 3. (Color online) LIS at ω=0.12 a.u. (full lines) whose calculation could be extended in shadow form to α_0 values below their materialization point (dotted lines), some as far as α_0=0. For the latter, the unperturbed states they are connected to have been indicated.

We show the results in Fig. 3 for the case of ω=0.12 and the consecutive LISs: (LIS 3;11), (LIS 5;13), (LIS 6;6), (LIS 7;7), (LIS 8;20). Only the last three LIS could be extended to α_0=0, where they originate (modulo ω) in the unperturbed states n=1, 6, and 5, respectively. In our computation we have retained typically N=21 equations (except at large α_0, where we have taken 25), achieving in general an accuracy of better than 0.1% for Re E, and better than 1% for Γ (except in the vicinity of the materialization thresholds).

To compare our accurate numerical Floquet results with the predictions of HIHFFT obtained in I, we have also carried out a computation of the expressions of the latter for the potential Eq. (1). HIHFFT expresses the real part of the quasienergy to first order as $\mathrm{Re}\, E^{(1)} \simeq W(\alpha_0) + \Delta W(\alpha_0, \omega)$, where $W(\alpha_0)$ is an eigenvalue of the *structure equation*

$$\left(\frac{1}{2}P^2 + V_0(\alpha_0; x)\right)u = W(\alpha_0)u, \tag{10}$$

and $\Delta W(\alpha_0, \omega)$ is given by I Eqs. (19) and (20). Γ is obtained from I Eq. (21). The numerical computation of these expres-

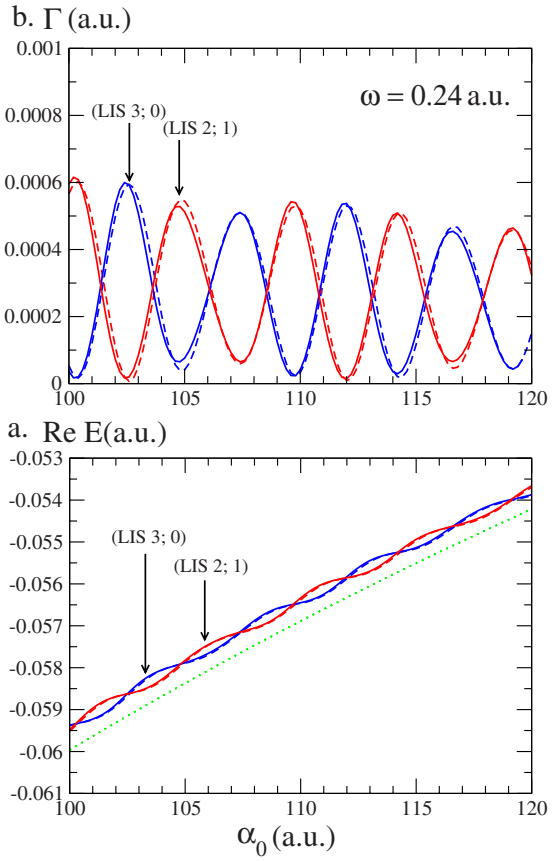

FIG. 4. (Color online) (a) Re E and (b) Γ for states (LIS 3;0) and (LIS 2;1) at ω=0.24 a.u., according to exact Floquet theory (full lines), and HIHFFT results (see text) (dashed lines). The dotted line in (a) represents the structure equation approximation, from Eq. (10).

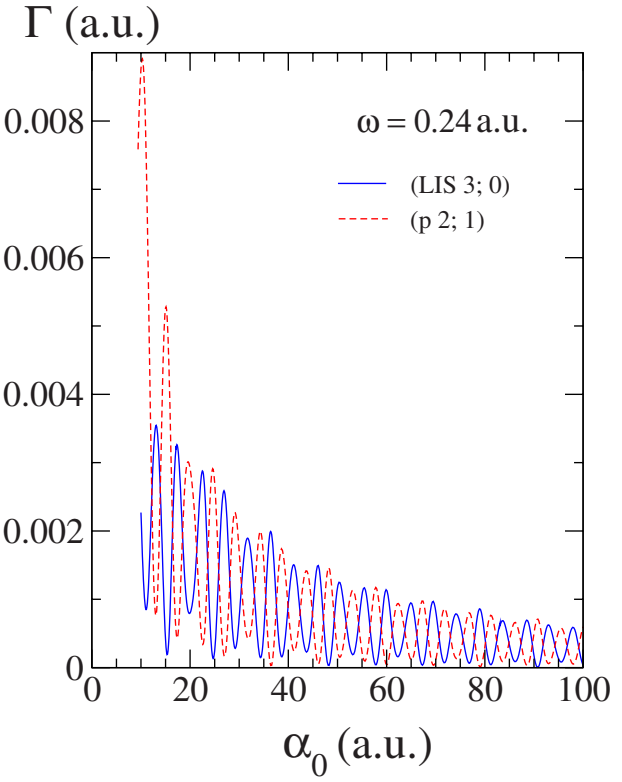

FIG. 5. (Color online) Floquet theory $\Gamma(\alpha_0)$ for states (LIS 3;0) and (LIS 2;1) at ω=0.24 a.u.; curves drawn as in Fig. 4.

sions was done along the lines described in [13], Sec. III. This is considerably simpler than the integration of the Floquet differential system.

III. HIHFFT, LARGE-α_0 ANALYTIC RESULTS

In I we have applied the general HIHFFT results to the 1D popular model with the soft-core Coulomb potential:

$$V(x) = -\frac{1}{\sqrt{a^2 + x^2}}. \tag{11}$$

The constant a was chosen a=1.414, so that the energy of the ground state was W_0=−0.500.

In the following we summarize the analytic HIHFFT results obtained for model Eq. (11) in the *large-*α_0, *all-*ω case. The details of the calculation are contained in I.

(1) The α_0 dependence of the eigenvalues of the structure equation (10) is, to a good approximation, given by

$$W(\alpha_0) \simeq [\lambda(\alpha_0)]^{-2}\mathcal{W}^{(0)}; \tag{12}$$

see I Eq. (63). Here, $\mathcal{W}^{(0)}$ is a constant of order 1, and $\lambda(\alpha_0)$ is given by I Eq. (61). $\lambda(\alpha_0)$ increases with α_0 slightly more slowly than $\alpha_0^{1/3}$, and $W(\alpha_0)$ decreases with α_0 slightly more slowly than $\alpha_0^{-2/3}$. The normalized dichotomous eigenfunctions corresponding to $W(\alpha_0)$ are

$$u^P(x) \simeq \frac{1}{\sqrt{2\lambda}}[v(x_-/\lambda) + (-1)^P v(-x_+/\lambda)], \tag{13}$$

where $v(\xi)$ is an eigenfunction of I Eq. (60).

(2) The dominant form of the first-order *energy correction* $\Delta E^{(1)}$, I Eqs. (96) and (97), is

$$\Delta W = \frac{\pi^2}{6}\frac{[f(0)]^2}{12a^2}[v(0)]^2\frac{1}{\alpha_0\lambda\omega^2} + (-1)^{P+1}\frac{\pi}{\alpha_0\lambda\omega}[v(0)]^2\sum_{m>0}\frac{(-1)^m}{m}\cos 2k_m\alpha_0[\mathcal{V}(k_m)]^2, \tag{14}$$

$$\Gamma = \frac{2\pi}{\alpha_0\lambda\omega}[v(0)]^2\sum_{m>0}\frac{1}{m}[1 + (-1)^{m+P}\sin 2k_m\alpha_0][\mathcal{V}(k_m)]^2. \tag{15}$$

Here, $\mathcal{V}(k)$ is the Fourier transform of the potential Eq. (1) above [17], $v(0)$ is the value of $v(\xi)$ at the origin, $f(0) = {}_2F_1(1/2, 1/2, 1; 1/2)$, a^2 is the constant contained in $V(x)$, and $k_m \simeq +\sqrt{2m\omega}$.

ΔW and Γ contain sums over m involving $\cos 2k_m\alpha_0$ and $\sin 2k_m\alpha_0$, respectively . These sums are dephased in α_0 by $\pi/2$ for P=0 and by $3\pi/2$ for P=1.

(3) Concerning the *Floquet components* $\phi_n^{(1)}(x)$, open channels correspond to $n>0$, closed channels to $n<0$. The x

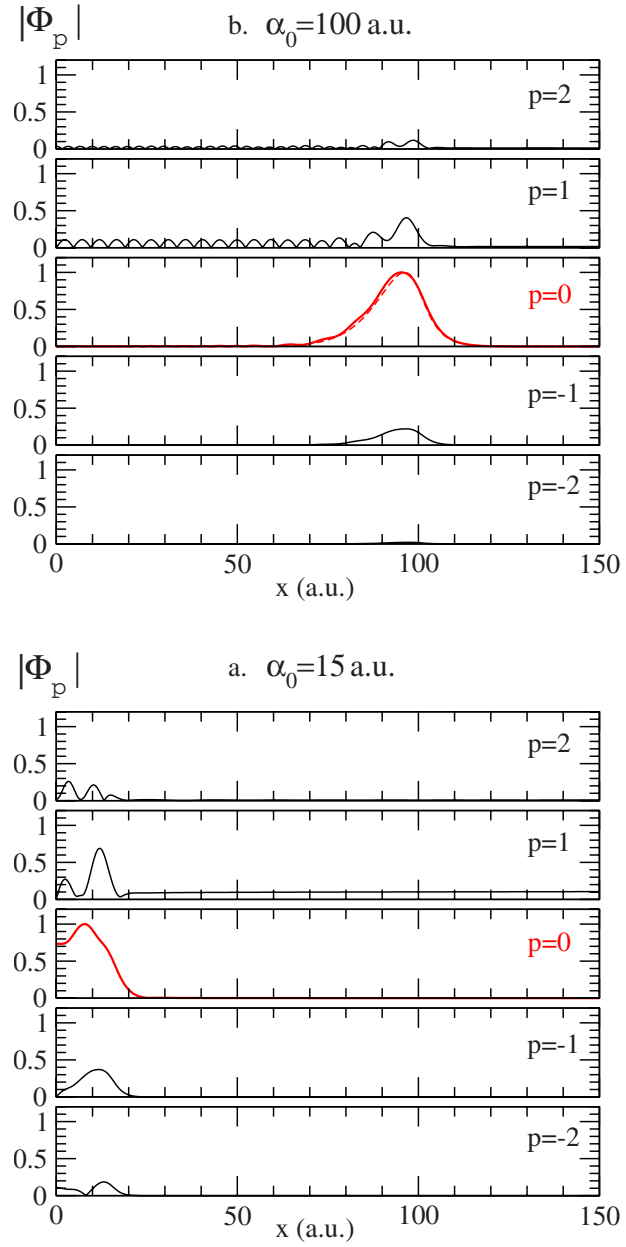

FIG. 6. (Color online) Modulus of Floquet components $|\phi_p(x)|$ of state (LIS 3;0) at $\omega=0.24$ a.u. and (a) $\alpha_0=15$, and (b) $\alpha_0=100$. The first open channel is set at $p=1$; the dominant channel isj $p=0$. Dichotomy has already set in by $\alpha_0=100$ in all closed channels.

axis has been divided into three intervals: interval A lies inbetween the lobes of the dichotomous atom; interval B covers the lobes; interval C lies outside the two lobes (for a more stringent definition of the intervals, see I, Sec. III C).

On *interval A*, for open channels $|\phi_n^{(1)}(x)|$ oscillates as $|\cos[k_n x+(P+n)\pi/2]|$ with frequency k_n. For closed channels it behaves as $\cosh|k_n|x$ (if $P+n=$even) or $|\sinh|k_n|x|$ (if $P+n=$odd), and hence increases exponentially when $|x|$ grows from 0 to α_0. All closed channels are dichotomous, just as for $n=0$.

On *interval B*, for open channels,

$$|\phi_n^{(1)}(x)|^2 \simeq \frac{1}{2\lambda k_n^2}\left[\frac{4}{k_n^2}\tilde{V}_0^2(x_-)v^2(x_-/\lambda) + \frac{4}{k_n}(-1)^{P+n}|I(-k_n)|\tilde{V}_0(x_-)v(x_-/\lambda) \times\sin\left(k_n(x_-+2\alpha_0)-\frac{\pi}{4}\right)+|I(-k_n)|^2\right], \quad (16)$$

where $I(-k_n)$ is given by I Eq. (90), and $\tilde{V}_0(x_-)$ by I Eq. (53). When the last term in the square brackets is small with respect to the first one, $|\phi_n^{(1)}(x)|^2$ has practically the same nodes as the dichotomous state $u^P(x)$ in the vicinity of the endpoint $+\alpha_0$ [recall Eq. (13)]. The smooth dependence on x of the first term is then *modulated* by the second term, with the same frequency k_n that $|\phi_n^{(1)}(x)|$ has on interval A; moreover, the amplitude of the oscillations is small. Note that $\tilde{V}_0(x_-)$ has no zeros.

For closed channels, on the other hand,

$$|\phi_n^{(1)}(x)|^2 \simeq \frac{2}{\lambda|k_n|^4}\tilde{V}_0^2(x_-)v^2(x_-/\lambda). \quad (17)$$

Now $|\phi_n^{(1)}(x)|^2$ has precisely the same nodes as $u^P(x)$. As opposed to the open channel case, there is no modulation.

On *interval C*, $|\phi_n^{(1)}(x)|$ is constant in x for open channels [18], and decays exponentially toward infinity for closed channels.

The analytical results derived above will help interpret the numerical Floquet results described in the next sections. Note that the potential Eq. (11) is slightly different from that in Eq. (1) used in our numerical Floquet computations. However, the numerical differences for the quasienergies, besides being small, are irrelevant for interpretation of the numerical Floquet theory.

IV. FLOQUET NUMERICAL RESULTS FOR QUASIENERGIES

Our Floquet calculations have been carried out at low photon energies $\omega=0.12$ and 0.24 ($\omega<|W_0|$). In the first case five photons are needed to ionize the system at low intensity, in the second case, three photons. The results for Re $E(\alpha_0)$ are shown as full lines in Figs. 1(a), 1(b), 2(a), and 2(b); see also Fig. 9 below. The quasienergies of the states have been shifted by the multiple of ω needed so that their Re $E(\alpha_0)$ fits in the first negative energy band, $-\omega<\mathrm{Re}\,E<0$. A superscript (q) indicates an upward shift of $q\omega$. Due to the Floquet redundancy mentioned in I, Sec. II A, these shifted quasienergies correspond to actual Floquet states, but with a different parity $(-1)^{P+q}$ than the original one $(-1)^P$. The quasienergies have been grouped according to the parity of the shifted states. The rationale for this grouping is that only same-parity Floquet states interact giving rise to ACs in the complex energy plane. Figures 1(a) and 2(a) contain the even states for $\omega=0.12$ and 0.24, respectively, and Figs. 1(b) and 2(b), the odd states. Only states that are physical within the energy band are shown. We shall refer to the representation of Re E as function of α_0 in these figures as Floquet maps.

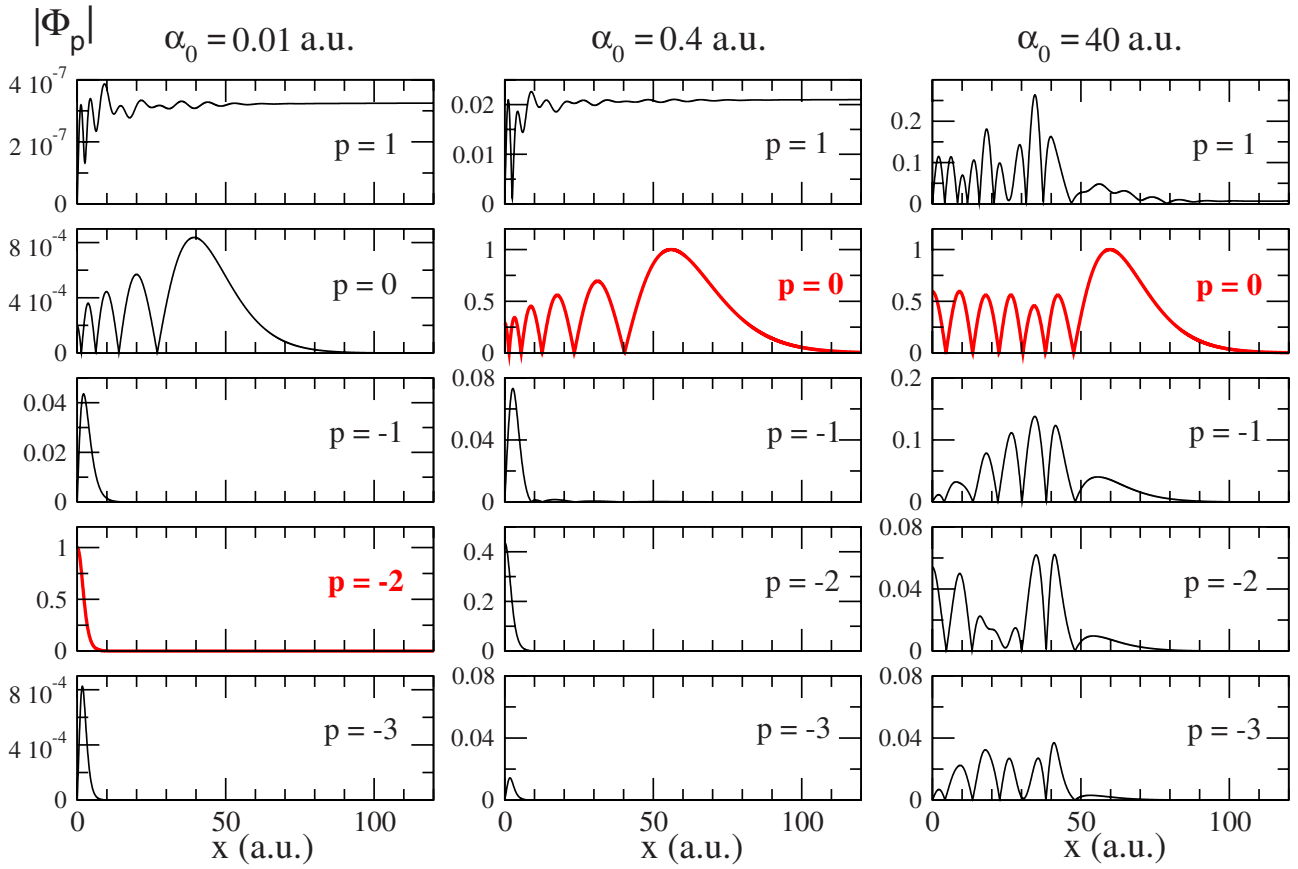

FIG. 7. (Color online) Modulus of Floquet components $|\phi_p(x)|$ of state $(0^{(2)};12)$, at ω=0.24 a.u. and α_0 as indicated. The first open channel is set at p=1. The dominant component is the heavier line (red in color). The set $\{|\phi_p(x)|\}$ is normalized such that the maximum of the dominant component is 1.

Also shown in these figures by dashed lines are the computed eigenvalues $W(\alpha_0)$ of the structure equation (10).

At low and intermediate α_0, Re $E(\alpha_0)$ has a rather contorted behavior due to numerous crossing and ACs. However, as α_0 increases this behavior calms down, and at large α_0, all Floquet Re $E(\alpha_0)$ settle on the eigenenergies of the structure equation, as predicted by HIHFFT. This occurs sooner for the higher frequency ω=0.24 than for ω=0.12, as anticipated [19].

Crossing and ACs occur when Re $E(\alpha_0)$ for the two states differ approximately by an integer number of ω (are equal modulo ω). In physical terms, this means that there is a resonance in the multiphoton ionization of the states; for a discussion of Floquet resonances; see, e.g., [10]. As opposed to the usual case of real eigenvalues of a Hermitian Hamiltonian which obey the von Neumann–Wigner noncrossing rule, quasienergies are complex and obey a generalized noncrossing rule: their trajectories in the complex energy plane cannot intersect at the same value of α_0. ACs in the complex plane can be characterized by a minimum of the distance between two quasienergies calculated at the same α_0, $d_{ij}(\alpha_0) \equiv |E_i(\alpha_0) - E_j(\alpha_0)|$. In general, at a narrow AC (sharp minimum of d_{ij}) either the Re $E(\alpha_0)$ can avoid each other, but then Im $E(\alpha_0)$ cross, or vice versa, Im $E(\alpha_0)$ avoid each other but then Re $E(\alpha_0)$ cross (there are also exceptions). Therefore, one cannot assess the behavior of the system at ACs on the basis of Floquet maps for Re E only; information on Im $E(\alpha_0)$ is needed in order to understand the whole picture [20]. A detailed discussion of diabatic paths and complex ACs for our model will be given elsewhere [21].

The overall behavior of the states, from low to large α_0, is reflected by the behavior of Re $E(\alpha_0)$, and can be categorized as follows. (I) Some states are physical at all α_0, i.e., Re $E(\alpha_0)$ starts from a field-free energy at α_0=0, stays in the energy band, and goes over into an eigenvalue of the structure equation at large α_0. (II) Other states start by being physical but at some α_0 become LSSs, i.e., Re $E(\alpha_0)$ starts from a field-free energy at α_0=0, stays in the energy band for a while, but then hits the lower or upper ω threshold, and disappears as a physical state because Eqs. (6) and (7) cannot be satisfied for all channels n. (III) Still other states are LISs, i.e., they start come into existence at some $\alpha_0 > 0$, and remain so beyond it, i.e., Re $E(\alpha_0)$ starts at the upper or lower thresholds of the energy band and remains in it. (IV) Finally, some of the LISs become LSSs at some higher α_0, i.e., Re $E(\alpha_0)$ appears in the energy band at some $\alpha_0 > 0$ but hits one of the thresholds afterward.

In order to keep track of this behavior, we have introduced a two-label notation $(n;\nu)$ for the states. For category I, the first label n stands for the field-free state in which the Floquet state originates at α_0=0, and the second label ν stands for the state of the structure equation to which it tends at large α_0; such are the states $(0^{(4)};8)$, $(2^{(1)};17)$, (4;4). (These and the following examples refer to the ω=0.12

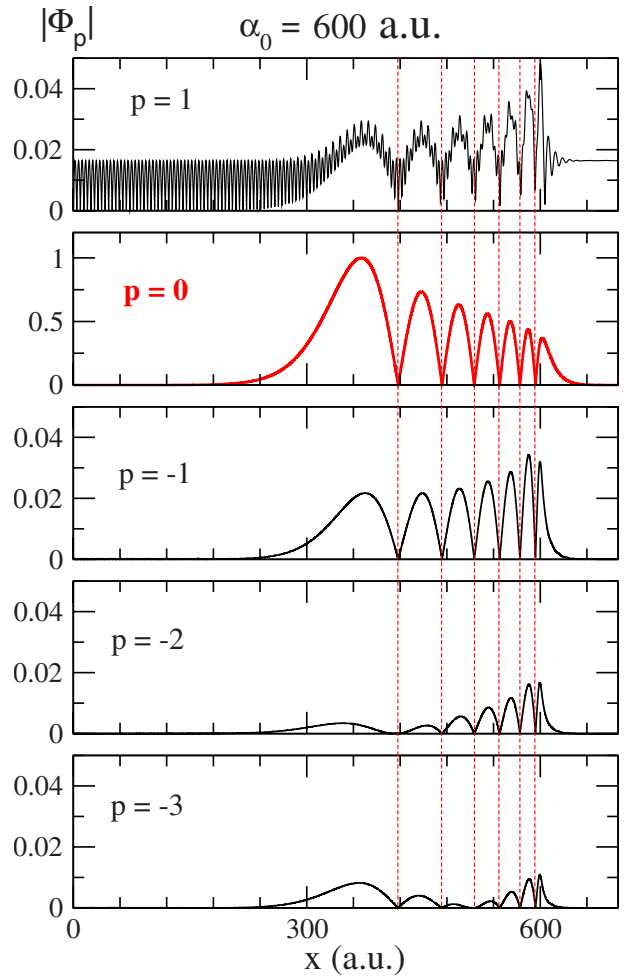

FIG. 8. (Color online) Same as Fig. 7, except that α_0=600. Vertical dashed lines were drawn to show the common location of the nodes.

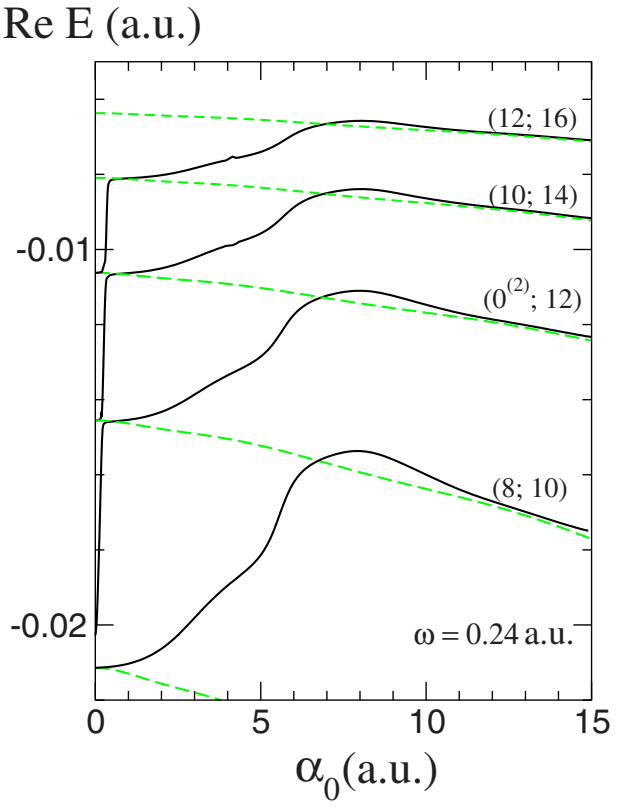

FIG. 9. (Color online) Detail of Fig. 1(a) for Re $E(\alpha_0)$ of even states at ω=0.24 a.u.

case.) Note that we label the n and ν states starting from 0. For category II, we designate states by (n; LSS), where n is the field-free state of origin; examples are ($1^{(2)}$; LSS) or (3; LSS). For category III, we write (LIS $p;\nu$), where p indicates the order of appearance of the LIS, and ν represents the large-α_0 state of the structure equation it tends to; examples are (LIS 12;0) or (LIS 11;1). Finally, for category IV, we write (LIS p; LSS); examples are (LIS 1; LSS) or (LIS 2; LSS).

As predicted by HIHFFT, at large α_0, Re $E(\alpha_0)$ as well as $W(\alpha_0)$, coalesce in even-odd pairs (even-odd degeneracy), albeit rather slowly. For example, at ω=0.12 the state (LIS 12;0) coalesces with (LIS 11;1), (LIS 10;2) with (LIS 9;3), etc. To illustrate in more detail the situation we show in Fig. 4(a) the coalescence of the states (LIS 3;0) and (LIS 2;1) at ω=0.24, according to exact Floquet theory and HIHFFT. Note first that the results of the two theories lie right on top of each other. The structure equation results for $W(\alpha_0)$ of the two states are coincident and shown by the dotted line in Fig. 4(a), which lies close to the actual results. An oscillatory dependence on α_0 is apparent for the Floquet and HIHFFT results Re $E(\alpha_0)$, the two coalescing energies oscillating with almost π difference of phase. This feature is explained by the analytic HIHFFT expression for the energy correction ΔW, Eq. (14), in which the oscillating term has opposite sign for the P=0 and P=1 states. Moreover, although the oscillating term contains the superposition of an infinity of frequencies $\cos 2k_n\alpha_0$, because of the rapid decrease with m of $[\mathcal{V}(k_m)]^2/m$, only few terms contribute effectively. This gives the oscillating contribution a nearly harmonic character.

We now turn our attention to $\Gamma(\alpha_0)$. A typical result at ω=0.24 is shown for the coalescent states (LIS 3;0) and (LIS 2;1) in Fig. 4(b) for a restricted α_0 range , and in Fig. 5 for an extended range. It is apparent from Fig. 5 that at large α_0, $\Gamma(\alpha_0)$ decreases with increasing α_0 on the average, which is per definition QS. The decrease is rather slow and oscillatory. Figure 4(b) contains also the HIHFFT result obtained for Γ via I Eq. (21), which compares rather well with the Floquet result. Note that the Γ's for the two states oscillate with opposite phases, in agreement with the analytic HIHFFT formula Eq. (15). Moreover, by comparing the exact Floquet and HIHFFT calculations for ΔW and Γ in Figs. 4(a) and 4(b), it is apparent that there is a $\pi/2$ phase difference between the oscillations of the latter for both states with P=0 and 1. Also this feature is borne out by the analytical results of Eqs. (14) and (15).

V. FLOQUET NUMERICAL RESULTS FOR WAVE FUNCTION

We now focus on the properties of the components $\{\phi_p(x)\}$ of the Floquet wave function. As noted in I, Sec.

II A, the $\phi_p(x)$ have parity, consecutive components having alternating parities. Hence it is sufficient to represent them for $x>0$. As the labeling of the components is arbitrary (i.e., the label $p=0$ can be placed at will because of the Floquet redundancy), we shall set in all cases the first open channel at $p=1$. As $\phi_p(x)$ are complex numbers, we shall represent for simplicity their modulus. The set $\{\phi_p(x)\}$ is defined by the differential system Eq. (2) only up to a constant factor. We have normalized it by imposing that the maximum value attained by the dominant component $|\phi_p(x)|$ be 1. In our figures we show the five most prominent components.

In Fig. 6 we consider the state (LIS 3;0) for $\omega=0.24$ and $\alpha_0=15$ and 100. At $\alpha_0=100$ it is the ground state of the atom; see Fig. 2(a). This agrees with the fact that its dominant component $p=0$ coincides with the ground state eigenfunction of the structure equation (shown as dotted in the figure), the other components being small. $\phi_0(x)$ clearly undergoes dichotomy when α_0 passes from 15 to 100, with the wave function concentrating in the vicinity of the end points $\pm\alpha_0$. However, dichotomy appears in all closed channels [e.g., $p=-1,-2$, in Fig. 6(b)]. In the open channels of Fig. 6(b) (e.g., $p=1,2$), $|\phi_p(x)|$ oscillates between the charge lobes ($|x|<\alpha_0$) like $|\sin k_p x|$ or $|\cos k_p x|$, depending on parity. In the vicinity of the end points $\pm\alpha_0$, $|\phi_p(x)|$ is strongly affected by channel coupling; see below. For $|x|>\alpha_0$, $|\phi_p(x)|$ becomes nearly constant. Note that the exponential blow-up of $|\phi_p(x)|$ imposed by the Floquet boundary conditions Eqs. (5)–(7) occurs at larger $|x|$ than shown in Fig. 6(b). All these features are predicted by the formulas derived analytically from HIHFFT (see Sec. III point 3).

We now focus on the true ground state of the system, labeled $(0^{(2)};12)$ in Fig. 2(a), and on the changes induced in its Floquet wave function when the intensity (α_0) grows from 0 to large values, such as 600, at $\omega=0.24$. [For a better vizualization of Re $E(\alpha_0)$ at low α_0 we refer to the map Fig. 9.] The components $|\phi_p(x)|$ are shown in Fig. 7 at $\alpha_0=0.01,0.4,40$, and in Fig. 8 at $\alpha_0=600$. The change is impressive.

At $\alpha_0=0.01$, since we have placed the first open channel at $p=1$, the dominant channel is $p=-2$, and three photons are needed to ionize. $\phi_{-2}(x)$ is nodeless and coincides essentially with the unperturbed ground state eigenfunction of the atom, the other components being small. At $\alpha_0=0.4$ the dominant component has moved to $p=0$ and has ten nodes. Due to the compression of the Re E spectrum [see Fig. 2(a)] only one photon is needed now for ionization. For $\alpha_0>0.4$ the dominant component stays at $p=0$, but by $\alpha_0=40$ it has acquired 12 nodes, which it maintains thereafter. Since the quasienergy settles on the $\nu=12$ eigenvalue of the structure equation, the dominant component $\phi_0(x)$ and the $\nu=12$ eigenfunction should coincide. Indeed, when superposed with the same normalization, at $\alpha_0=600$ the two functions are indistinguishable at the graphical level.

The numerical results show that changes in the Floquet wave function occur gradually between ACs, and suddenly at ACs. Let us illustrate this for the case of $(0^{(2)};12)$ considered above. The state is involved in two ACs (see Fig. 9): one occurs over the range $0.15\lesssim\alpha_0\lesssim0.25$, the other one occurs over the range $4\lesssim\alpha_0\lesssim12$. The α_0 values of these ACs lie between the values at which the components are shown in Fig. 7. In both cases it is the Re $E(\alpha_0)$ that avoid each other.

The AC at $0.15\lesssim\alpha_0\lesssim0.25$ is narrow and can be described in terms of the two-state approximation of the Floquet system Eq. (2). Similarly to the case of a Hermitian Hamiltonian, there is a swap of structure between the dominant components of the interacting states. By this we mean that, if the Floquet states (a) and (b) entering an AC have dominant components $\phi_p(x)$ and $\psi_q(x)$, respectively, beyond the AC they will have dominant components $\psi_q(x)$ and $\phi_p(x)$, respectively. Thus, with reference to Figs. 6 and 8, the state $(0^{(2)};12)$ enters the AC with dominant component $p=-2$ having zero nodes, as it started at $\alpha_0=0$. Its interaction partner (10;14) starts out at $\alpha_0=0$ with dominant component $p=0$ having ten nodes. Beyond the AC, the dominant component of $(0^{(2)};12)$ is $p=0$ and has ten nodes (see Fig. 7), while that of (10;14) is at $p=-2$ and has zero nodes (not shown). A similar swapping holds for the other states shown in Fig. 9 [with the exception of (8;10)], at a slightly different α_0.

The second AC for $(0^{(2)};12)$, occurring over the range $4\lesssim\alpha_0\lesssim12$, is part of a multistate AC that is not amenable to a sum of binary interactions. Indeed, all states shown in Fig. 9 (as well as higher ones, not shown) participate in this AC, in the following way: the nodal structure of the dominant component is transferred only from the higher state to the lower state it interacts with, and not vice versa. Thus, the structure of the dominant component of $(0^{(2)};12)$, which when entering the AC is characterized by $p=0$ and 10 nodes (see Fig. 7), is transmitted to (8,10), not shown. The structure of the dominant component of the next higher state (10;14), characterized at the time it enters the AC by $p=0$ and 12 nodes, is transmitted to the dominant component of $(0^{(2)};12)$, characterized by $p=0$ and 12 nodes (see Fig. 7), etc. Thereafter, for growing α_0, the dominant component of $(0^{(2)};12)$ gradually settles on the eigenfunction $\nu=12$ of the structure equation, while the other components vanish. A detailed analysis of the situation will be presented elsewhere [21].

Finally, let us point out a noteworthy feature in the structure of the components $\phi_p(x)$ at large α_0. We illustrate the situation again by the behavior of $(0^{(2)};12)$ shown in Fig. 8. On the x intervals lying outside or between the charge lobes, the situation is similar to that in Fig. 6 and we shall not recall it. Of present interest is the interval covering the charge lobes (called interval B in Sec. III at point 3). At $\alpha_0=600$ the structure of the dominant component $\phi_0(x)$ has settled on the $\nu=12$ eigenfunction of the structure equation. Note how the nodes of the dominant component $\phi_0(x)$ are replicated in all closed and open channels. For better vizualization we have drawn in Fig. 8 vertical dashed lines passing through the nodes. Whereas the nodes for closed channels are replicated to within the graphical accuracy of the vertical lines, for open channels (e.g., $p=1$) there are, strictly speaking, no nodes, but rather deep minima. In addition, for open channels, the components are modulated with the frequency existing on interval A, between the lobes. Also these features are predicted by the analytic formulas of Sec. III point 3 [see Eqs. (16) and (17)]. Thus, the dichotomous strucure of the dominant component is present in all closed channels and affects also the open channels.

VI. CONCLUSIONS

We have made a comprehensive computation of the quasienergies of a dynamical system, from low to large α_0 ($0<\alpha_0<100$), for the first 18 low-lying states, at the low frequencies $\omega=0.12$ and 0.24 (smaller than the unperturbed binding energy $|W_0|=0.500$). We have presented graphs for the α_0 dependence of the energies of the states in the field $W(\alpha_0)=\mathrm{Re}\,E$ (Floquet maps) and their ionization rates $\Gamma(\alpha_0)$. An intricate behavior of $W(\alpha_0)$ at low α_0 was revealed, with many crossings, avoided crossings, and Floquet states materializing or disappearing at ω energy thresholds. At large α_0, however, the uneventful pattern encountered at high frequencies is regained, in which the levels tend monotonically to zero modulo ω (i.e., the binding energies of all states vanish). Changes in the components of the Floquet wave function were followed from low to large α_0. They were related to the ACs of the quasienergies.

We have also compared the accurate Floquet results to HIHFFT. To this end, we have first computed the general expressions of HIHFFT for the 1D model. We found quite good agreement, within the expected errors, confirming that HIHFFT is fully capable of describing the low-frequency regime. Moreover, the analytic formulas derived from HIHFFT for the large-α_0 limit, presented in Sec. III, give a transparent interpretation of the numerical Floquet results. In particular, we have confirmed the fact that QS and dichotomy can occur at any ω, provided that the field strength E_0 (or α_0) is sufficiently high.

The single-state Floquet theory results obtained, and in particular the maps, offer the possibility of visualizing the evolution of the atom under the influence of *laser pulses*, for which the field amplitude rises from zero to a peak value and returns to zero, i.e., we are dealing with a time-dependent $\alpha_0(t)$. Indeed, multistate Floquet theory expresses any wave packet as a superposition of individual states. As, in many instances, at some time only one of these states is preferentially populated, the evolution of the wave packet can be visualized by a point on the corresponding $W(\alpha_0)$ curve of the map. The trajectories of high probability inferred from the map, the diabatic paths, are instrumental in predicting the evolution of the atom and, alternatively, in steering it in desired directions using adequate pulses. This kind of analysis will be developed elsewhere [21].

ACKNOWLEDGMENTS

This work was partially supported by the National Science Foundation through a grant to ITAMP. Two of us (M.G. and I.S.) would like to thank A. Dalgarno for his hospitality there.

[1] M. Gavrila, J. Phys. B **35**, R147 (2002).
[2] M. Gavrila and J. Z. Kaminski, Phys. Rev. Lett. **52**, 613 (1984).
[3] M. Gavrila, in *Atoms in Intense Laser Fields*, edited by M. Gavrila (Academic, San Diego, 1992), p. 435.
[4] M. Gavrila, I. Simbotin, and M. Stroe, preceding paper, Phys. Rev. A **78**, 033404 (2008).
[5] A preliminary account of this work was given by I. Simbotin, M. Stroe, and M. Gavrila, Laser Phys. **14**, 482 (2004).
[6] R. M. Potvliege and S. Vucic, Phys. Rev. A **74**, 023412 (2006).
[7] J. C. Wells, I. Simbotin, and M. Gavrila, Laser Phys. **7**, 525 (1997).
[8] J. C. Wells, I. Simbotin, and M. Gavrila, Phys. Rev. A **56**, 3961 (1997).
[9] H. C. Day, B. Piraux, and R. M. Potvliege, Phys. Rev. A **61**, 031402(R) (2000).
[10] R. M. Potvliege and R. Shakeshaft, Phys. Rev. A **40**, 3061 (1989).
[11] J. C. Wells, I. Simbotin, and M. Gavrila, Phys. Rev. Lett. **80**, 3479 (1998); **82**, 665 (1999).
[12] J. C. Wells, I. Simbotin, and M. Gavrila, in *Multiphoton Processes*, edited by L. F. DiMauro, R. R. Freeman, and K. C. Kulander, AIP Conf. Proc. No. 525 (AIP, Melville, NY 2000), p. 89.
[13] M. Marinescu and M. Gavrila, Phys. Rev. A **53**, 2513 (1996).
[14] I. Simbotin (unpublished).
[15] K. Smith, *The Calculation of Atomic Collision Processes* (Wiley, New York, 1971).
[16] This explains the reason for introducing the exponential $\exp[-(x/a)^2]$ under the square root of Eq. (1). It has the effect of reducing the distance at which the potential becomes purely Coulomb.
[17] We define the Fourier transform of the potential similarly to Eq. (4).
[18] In our approximation, see I Eqs. (81) and (82), there is no exponential blow-up at infinity in the open channels.
[19] The analytic formula I Eq. (63) fits excellently the numerical results for $W(\alpha_0)$, to less than 1% error, although it pertains to potential Eq. (11) and not Eq. (1), and the corrective term $\mathcal{W}^{(1)}(\alpha_0)$ was not taken into account. This is because at large α_0 the eigenvalues of the two potentials are practically identical and $\mathcal{W}^{(1)}(\alpha_0)$ may be small.
[20] "Complete" Floquet maps, showing both $\mathrm{Re}\,E=W$ and $\mathrm{Im}\,E=-(\Gamma/2)$, have been introduced by J. C. Wells, I. Simbotin, and M. Gavrila, Phys. Rev. Lett. **80**, 3479 (1998); see Figs. 1 and 2 there, in which Γ is represented as the width of the energy W. The cases considered were the same as shown here in Figs. 1(a), 1(b), 2(a), and 2(b), but limited to $\alpha_0<4$.
[21] M. Stroe, I. Simbotin, and M. Gavrila (unpublished).